Supporting Information

Probing Adsorption Configuration of Methanol at Charged Interface by Nonlinear Spectroscopy

Caihe Liu[†,‡], Xujin Qin[†,‡], Changhui Yu[†,‡], Yuan Guo[†,‡], Zhen Zhang*[†,‡]

†Beijing National Laboratory of Molecular Sciences, State Key Laboratory of Molecular Reaction Dynamics, CAS Research/Education Center for Excellence in Molecular Sciences, Institute of Chemistry, Chinese Academy of Sciences, Beijing 100190, China

‡University of the Chinese Academy of Sciences, Beijing 100049, China

Contents

1. SFG spectra of methanol at air/electrolyte aqueous interface

The ssp spectra with an exposure time of 3 min and the SFG spectra of the quartz were collected (Figure S1(a) and S1(b)). The spectra and fitting results of 3 min were consistent with the results of 10 min (Table S4 and S5), that is, the oscillator strength of $CH_{3,SS}$ decreased at the surfaces of 0.1 M $NaClO_4$ solution and 0.1 M $HClO_4$ solution compared with the pure water surface. The quartz spectra before and after the experiment were almost exactly the same, indicating that the laser was stable during experiments, and the results are reliable and repeatable.

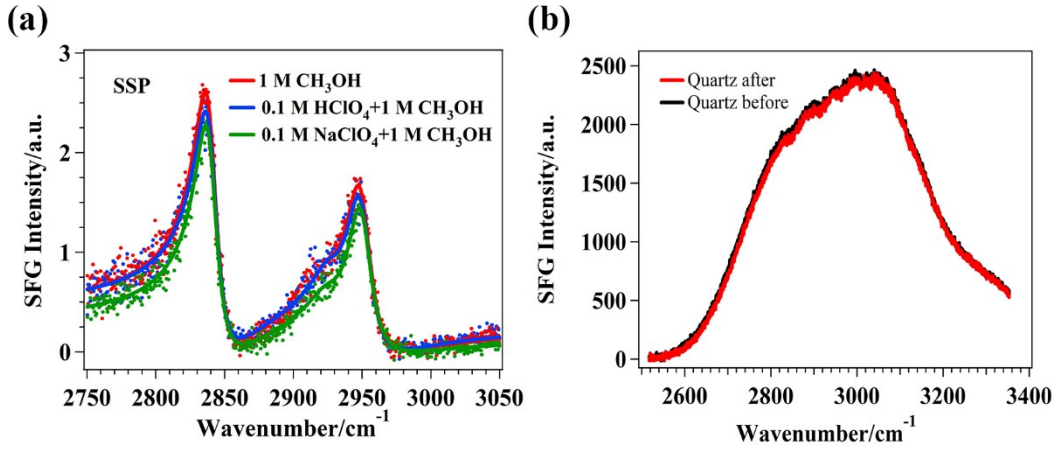

Figure S1. The SFG spectra of 1 M CH_3OH, 1 M CH_3OH+0.1 M $HClO_4$ and 1 M CH_3OH+0.1 M $NaClO_4$ solutions. (a) The exposure time of all spectra was 3 min. Dots are experimental data; the solid lines are fitted lines. (b) The SFG spectra of quartz before and after collecting three methanol solutions.

2. SFG spectra of the electrolyte solution surface

We used SFG spectra to check the purity of $NaClO_4$ and $HClO_4$ in 0.1 M $NaClO_4$ and $HClO_4$ electrolyte solution and pure water, with an exposure time of 10 min (Figure S2(a)). All SFG responses from the surface were silent in the C-H region and consistent with the SFG spectrum of salt baked at around 500 °C for more than 6 hours[1]. This indicates that there are no organic surface active impurities in the aqueous solution. Moreover, the SFG spectra of methanol molecules at the surfaces of pure water, 0.1 M $HClO_4$ and 0.1 M $NaClO_4$ electrolyte solution were also measured (Figure S2(b)). The

oscillator strength variation of $CH_{3,\,SS}$ was consistent with Figure 1(a) (Table S7).

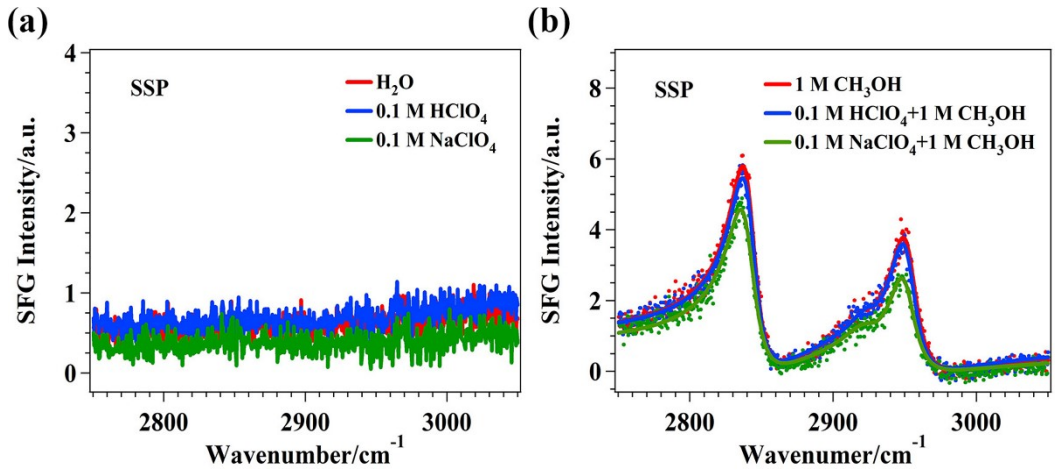

Figure S2. (a) The SFG spectra of air/water and electrolyte solution interface. (b) The SFG spectra of 1 M CH_3OH, 1 M CH_3OH+0.1 M $HClO_4$ and 1 M CH_3OH+0.1 M $NaClO_4$ solutions. The exposure time of all spectra in (a) and (b) was 10 min. The solid lines are fitted lines.

3. Laser-induced thermal effect

The effect of laser heating can be estimated by the local temperature at air/liquid interface. According to Bonn's work[2], the Lambert absorption coefficient $\alpha(\lambda)$ is expressed as:

$$\alpha(\lambda) = 4\pi k(\lambda)/\lambda \quad \text{(S1)}$$

where, k(λ) is the imaginary part of refractive index and λ is the wavelength of light. The molar fraction of methanol in 1 M methanol solution is 0.018. Therefore, the parameters of 1 M methanol solution are approximately the same as those of water. For the center wavelength of IR beam at the 2900 cm^{-1}, the k of water is about 0.013 [3]. From the Eq. (S1), we obtain $\alpha(\lambda) = 47375\ m^{-1}$.

The penetration depth d of IR beam can be calculated according to the follow equation:

$$I = I_0 \times e^{-\alpha * d} \quad \text{(S2)}$$

where I_0 is original average laser energy, I is the average absorbed energy in the interfacial region where 50% of the IR light is absorbed from the laser pulse. Then, one can calculate that the penetration depth d at 2900 cm^{-1} is 14.6 μm.

The single pulse temperature jump can be expressed as:

$$T = \frac{I}{m \times C} = \frac{I}{\rho \times \frac{\pi w^2}{4} \times d \times C} \tag{S3}$$

here, ρ and C is the density and heat capacity of the solution. The beam waist *w* of IR beam is about 200 μm. The single pulse energy of IR beam we used is about 7 μJ at the sample interface. Hence,

$$T = \frac{7 \times 10^{-6}\,(J) \times 0.5}{1000\,(kg/m^3) \times \frac{\pi \times (200 \times 10^{-6}\,m)^2}{4} \times 14.6 \times 10^{-6}\,(m) \times 4200\,(J/kg \cdot K)}$$

$$T = 1.8\,K$$

The thermal relaxation time (τ) is the time required for the temperature rise of a heated area to decrease by 37% [4]:

$$\tau = \frac{d^2}{4\alpha} \tag{S4}$$

where, d is the penetration depth and α is thermal diffusion coefficient. The thermal diffusion coefficient of water is 1.4×10^{-7} m^2/s [5]. As a result, $\tau = 0.38\,ms$. The temperature resulting from single pulse heating decreases to 0.67 K within a time period of 0.38 ms. The repetition rate of the laser is 1 kHz, which implies that the pulse interval between two laser shots is 1 ms. From this it can be estimated that the temperature caused by the single pulse heating is most likely negligible before the arrival of the second pulse.

Furthermore, Shen et al.[5] estimated that at a wavelength of 2.95 μm, when the laser pulse has a beam radius of 75 μm and an absorption length of 0.79 μm, the surface temperature rise at the irradiation center of the air/water interface remains at 3.0% after 1 ms by solving both analytically and numerically the heat diffusion equation. By using this parameter, the temperature resulting from single pulse heating decreases to 0.05 K before the arrival of the second pulse. Considering that the increasing temperature is inversely proportional to the ratio of the beam radius to the penetration depth, the

temperature caused by the single pulse heating in our work is less than 0.05 K before the arrival of subsequent pulse.

In order to remove the possible laser heating effect, the sample cell we used in this experiment is placed on a rotation stage (model No. PR50CC; Newport, Stratford, CT) operated by a motion controller (model No. XPS-Q4; Newport) with a fixed rate of 10°/s during the measurements. As shown in Figure S3(a), the laser spot is about 1 cm away from the sample cell center, then the sample cell moves about 0.002 mm in 1 ms. Since the beam waist *w* of IR beam is about 200 μm, the subsequent IR laser spot almost coincides with the first IR laser spot (Figure S3(b)). If the temperature caused by the single pulse heating does not completely reduce to zero before the subsequent pulses reach the interface, the accumulated thermal effect will occur. As shown in Figure S3(b), the first IR pulsed laser spot moves as the sample cell rotates. Take the center of the first IR pulse laser spot as a reference, until the 50th pulse reaches the interface after 50 ms, at which time the sample cell moves 0.1 mm, which is just the radius of the IR laser spot, that is, the edge of the 50th IR pulsed laser spot coincides with or is tangent to the center of the first IR pulsed laser spot. At this time, the thermal effect accumulated in the center of the first pulse laser spot is the largest. As mentioned above, if the temperature resulting from single pulse heating is 0.05 K before the arrival of the second pulse, the maximum IR laser-induced temperature at interface is 2.5 K.

According to the above calculation, it can be seen that the local temperature rise induced by single pulse or accumulated heating is about 1.8 K or 2.5 K. Such small heating effect is negligible with sample rotation during our measurement.

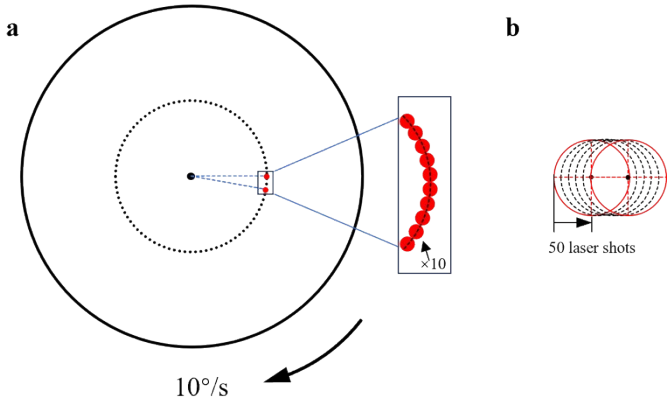

Figure S3. (a) Laser spot trajectory diagram during measurements. During the measurements, the laser spot is about 1 cm away from the sample cell center. The dashed circle represents laser spot trajectory diagram during measurements. The solid circle represents sample cell. The small solid red dots represent the position of the IR laser spot before and after 1 s. The IR laser spot in the large rectangular frame on the right is magnified 10 times compared to the rectangle on the left. (b) The IR laser spots on the sample cell surface during rotation. The red circle on the left is the first IR laser spot. The red circle on the right is the 50th IR laser spot.

On the other hand, the single pulse energy of IR beam is about 7 μJ at the sample interface. In the many SFG studies related to methanol at air/liquid interface in the literatures, the single pulse energy of broadband IR beam is 10 μJ in Allen's work[6]; the single pulse energy of broadband IR beam is 5.4 μJ in Lu's work[7]; the single pulse energy of ps IR beam is 0.15 mJ in Shen's work[8]; the single pulse energy of ps IR beam is about 200 mJ in Wang'work[9, 10], Kim'work[11] and Lu'work[12]. Although the IR pulse energy in these works is not the same, the obtained methanol SFG spectra are similar to those in these works and ours. Therefore, the single pulse energy of IR beam used in the experiment should have no effect on methanol.

Based on the above laser thermal effect calculations and other SFG studies related to methanol at air/liquid interface, we think that the IR laser beam has negligible effect on methanol and SFG spectra.

4. The orientation angle analysis of interfacial methanol

To compare the rationality of the calculation results of orientation angle of CH_3, the 3 M methanol aqueous solution and neat methanol were also measured. The orientation angles of CH_3 were calculated using data from Table S4 and Table S8. The refractive index in the orientation analysis are: $n_1(\omega) = n_1(\omega_1) = n_1(\omega_2) = 1.0$, $n_1(\omega) = n_1(\omega_1) = 1.33$, $n_2(\omega_2) = 1.4_3$, $n' = n_2\sqrt{(n_2)^2 + \frac{5}{(4(n_2)^2 + 2)}}$ [13]. For methanol, the Raman depolarization ratio of methanol at ~2837 cm^{-1} is 0.014, which was

experimentally measured in Colles's work[14]. Then, the hyperpolarizability ratio R can be obtained by Raman depolarization ratio ρ according to the expression proposed by Eisenthal et al.[15]:

$$\rho = \frac{3}{4 + 5\left(\frac{1+2R}{R-1}\right)^2} \quad \text{(S5)}$$

Here, the value of R=1.7 is frequently used to calculate the orientation angle of methyl at interface[9, 12, 16, 17]. Moreover, the R values have recently been measured again and are still around 1.7 for the methanol CH_3-ss at different concentrations[12]. Therefore, in our study we also used R=1.7 to calculate the orientation angle of methyl.

The orientation angle of CH_3 at the surface of neat methanol solution was 26.4°±0.1° (Table S1), which is consistent with the previously reported experiments[16, 18, 19] and molecular dynamics simulation results[20]。 The orientation angles of the 3 M and 1 M methanol solutions were very close, which indicates that the different exposure time has no effect on the CH_3 orientation angle of interfacial methanol.

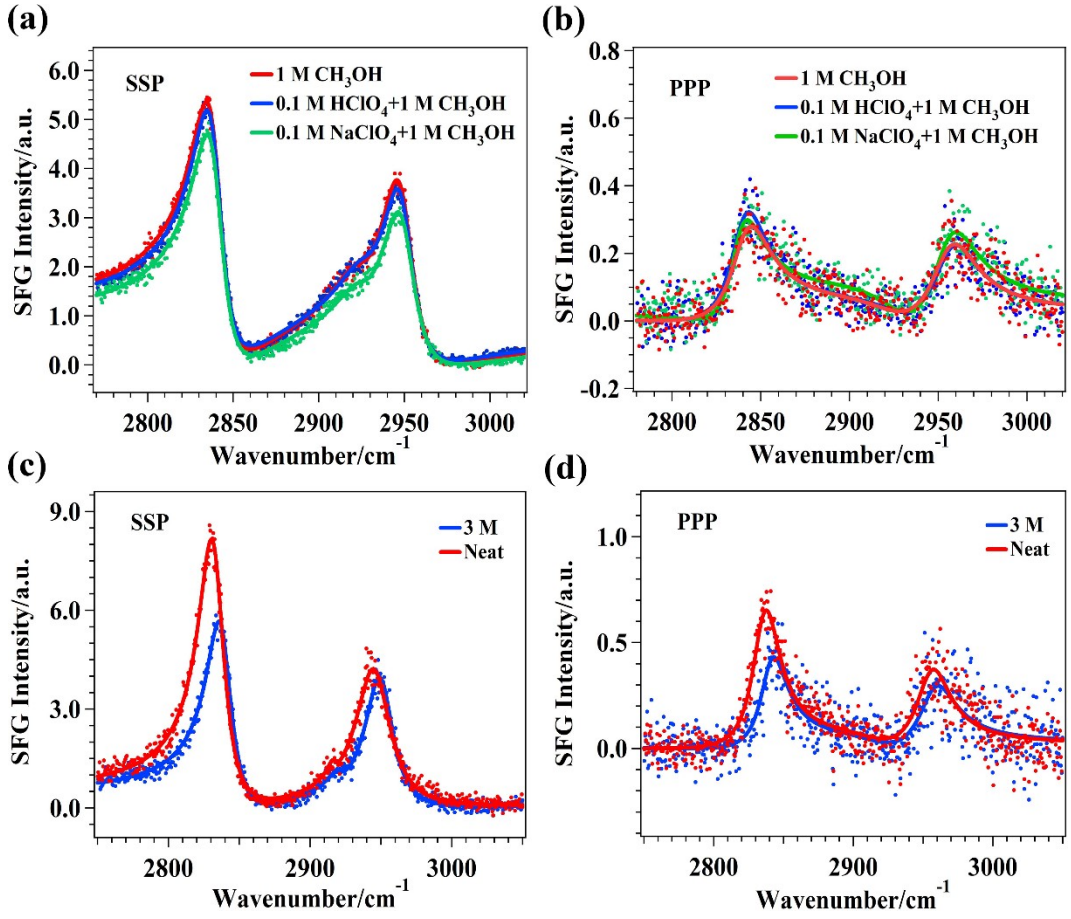

Figure S4. (a) and (b) The SFG spectra of 1 M CH_3OH, 1 M CH_3OH+0.1 M $HClO_4$

and 1 M CH_3OH+0.1 M $NaClO_4$ solutions. The exposure time of all spectra was 10 min. Figure S3(a) is Figure 1(a) in the main text. (c) and (d) The SFG spectra of 3 M CH_3OH and neat methanol, the exposure time of all spectra was 2 min. Dots are experimental data; the solid lines are fitted lines.

Table S1. The CH_3 orientation angles of interfacial methanol.

Liquid	θ (Degree)
Neat CH_3OH	26.4±0.1
3 M CH_3OH	28.8±0.1
1 M CH_3OH	27.9±0.1
0.1 M $HClO_4$+1 M CH_3OH	21.5±0.2
0.1 M $NaClO_4$+1 M CH_3OH	43.4±0.1

5. The HD-SHG measurement at the air/aqueous interface

The amplitude (E_{sig}) and phase (φ_{sig}) of the sample SHG signal can be obtained by fitting the interference pattern with the following equation[21-23]

$$I_{SHG} = I_1 + Acos(fx + \varphi_{fit}), \quad \text{(S6)}$$

where x is the stage position. I_1, A, f, and φ_{fit} are the fitting parameters. The changes of the φ_{fit} originates from changes of φ_{sig}.

Table S2. The fitting parameters of Figure 3(c).

liquid	I_1	A	f	φ_{fit}	φ_{sig}
H_2O	33.6±0.4	15.1±0.6	6.85	118.9°±0.04°	0±0.04°
0.1 M $HClO_4$	31.5±0.4	17.5±0.6	6.85	125.2°±0.03°	6.3°±0.05°
0.1 M $NaClO_4$	36.2±0.5	16.2±0.7	6.85	112.6°±0.04°	-6.3°±0.06°

6. Surface tension experiment

The surface tension measurement was performed using surface tensiometer (Shanghai Fangrui QBZY series). Each set of data is the average result of six tests.

Table S3 shows the surface tension of electrolyte aqueous solution with and without methanol. The surface tension of 0.1 M $HClO_4$ electrolyte solution decreased relative to the surface tension of pure water, while the surface tension of 0.1 M $NaClO_4$ electrolyte solution increased relative to the surface tension of pure water, which was consistent with the reported relative change of surface tension of $HClO_4$ and $NaClO_4$ electrolyte solutions[24]. The reliability of the experimental method and data is verified. Compared to pure electrolyte solution, the surface tension of 0.1 M $HClO_4$ +1 M CH_3OH and 0.1 M $NaClO_4$ +1 M CH_3OH solutions decreased after adding methanol. Importantly, among these six liquids, the surface tension of 0.1 M $NaClO_4$ electrolyte solution was the largest, and the surface tension of 0.1 M $NaClO_4$ +1 M CH_3OH solution was smallest, indicating that methanol has the highest relative number density at the interface of 0.1 M $NaClO_4$ electrolyte solution. Through quantitative analysis, the surface tension of 0.1 M $NaClO_4$, pure water and 0.1 M $HClO_4$ solution decreased by 9%, 8% and 8% respectively after adding methanol, which makes clear that the number density of the interfacial methanol at the surface of 0.1 M $NaClO_4$ solution was largest. Due to the enrichment of H_3O^+ and ClO_4^- ions at the air/aqueous interface, the number density of interfacial methanol at the surface 0.1 M $HClO_4$ solution was actually less than that of pure water interface. Therefore, methanol has the highest relative number density at the 0.1 M $NaClO_4$ electrolyte solution interface and methanol has the lowest relative number density at the 0.1 M $HClO_4$ electrolyte solution interface.

Table S3. The surface tension data. The error is the average deviation of each experimental measurement.

Solution	Surface Tension (mN/m)
Ultrapure water	71.06±0.05
0.1 M $HClO_4$	70.68±0.07
0.1 M $NaClO_4$	71.21±0.05
1 M CH_3OH	65.19±0.03

0.1 M $HClO_4$ +1 M CH_3OH	64.72±0.06
0.1 M $NaClO_4$ +1 M CH_3OH	64.44±0.09

7. SFG spectra of methanol at air/electrolyte aqueous interface in O-H region

As shown in Figure S5, compared to the 1 M CH_3OH surface, the peak intensity of strong hydrogen bonded structure also increased at the surface of 1 M CH_3OH+0.1 M $HClO_4$ solution and decreased at the surface of 1 M CH_3OH+0.1 $NaClO_4$ solution. We found that the oscillator strength of the strong hydrogen bond obtained by global fitting was always the biggest at 1 M CH_3OH+ 0.1 M $HClO_4$ solution surface, and the weakest at 1 M CH_3OH+ 0.1 M $NaClO_4$ solution surface, regardless of whether two peaks or three peaks were used for global fitting. This is also the case for the global fitting of hydrogen bond spectra on the surface of pure electrolyte solutions. Therefore, the surface potential does exist on the surface of the pure electrolyte solution. In addition, the PPP SFG spectra in the O-H region is very weak which lacks distinct spectral features (Figure S7).

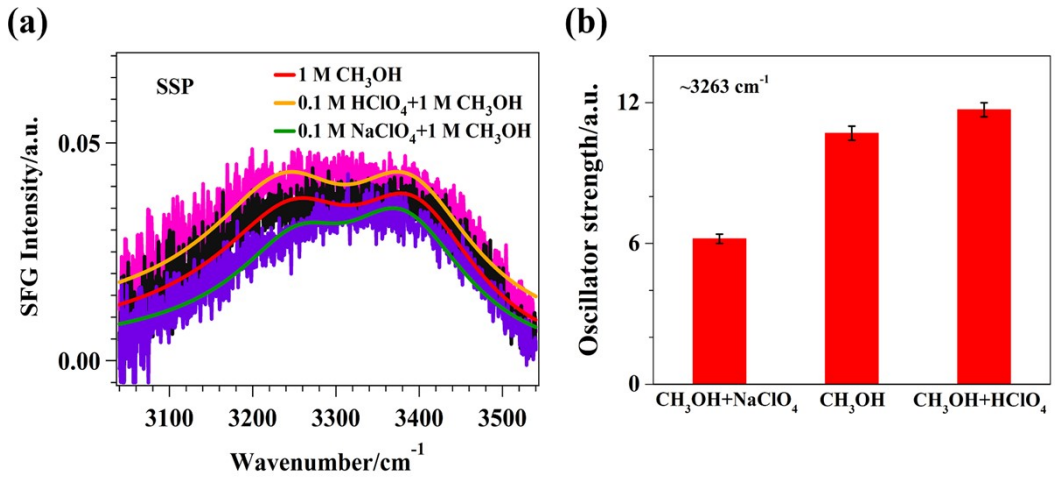

Figure S5. (a) The SFG spectra of 1 M CH_3OH, 1 M CH_3OH+0.1 M $HClO_4$ and 1 M CH_3OH+0.1 M $NaClO_4$ solutions in the O-H region. The exposure time of all spectra was 10 min. Dots are experimental data; the solid lines are fitted lines. The data of 1 M CH_3OH+0.1 M $HClO_4$ solution has been adjusted by 0.005 to enhance contrast. (b) The oscillator strength of peak at ~3263 cm^{-1} in (a). The data and error bars were obtained from global fitting using Eq. (1) (listed in Table S6).

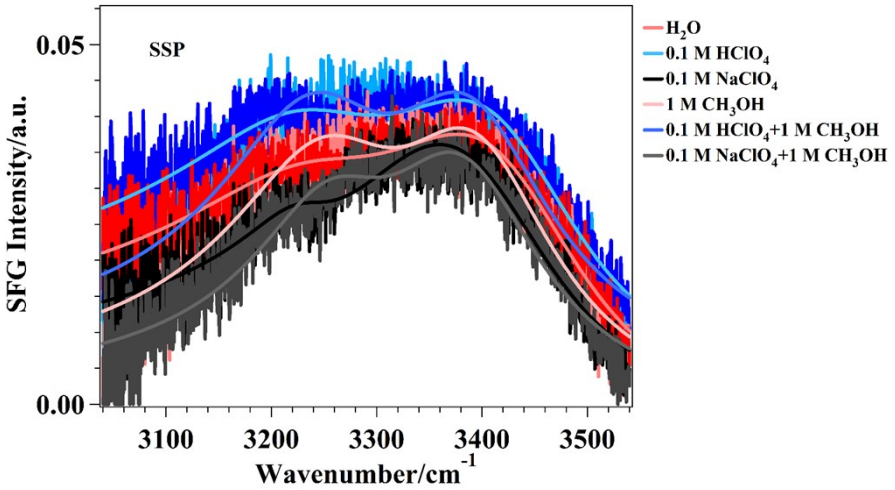

Figure S6. The SFG spectra of 0.1 M $NaClO_4$, pure water, 0.1 M $HClO_4$ solution, 1 M CH_3OH, 1 M CH_3OH+0.1 M $HClO_4$ and 1 M CH_3OH+0.1 M $NaClO_4$ solutions in the O-H region. The data is same in Figure 3(a) and Figure S5. The data of 0.1 M $HClO_4$ and 1 M CH_3OH+0.1 M $HClO_4$ solution has been adjusted by 0.005 to enhance contrast. The data and fitting lines for aqueous solutions containing methanol are lighter in color.

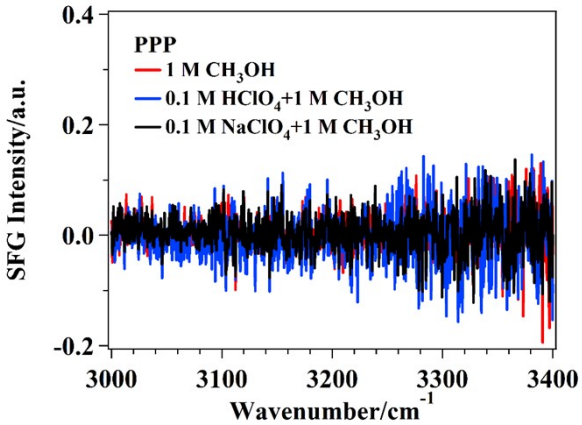

Figure S7. The SFG spectra of 1 M CH_3OH, 1 M CH_3OH+0.1 M $HClO_4$ and 1 M CH_3OH+0.1 M $NaClO_4$ solutions in the O-H region under PPP polarization combination. The exposure time of all spectra was 10 min.

8. The effect of methanol evaporation on SFG spectra

The evaporation of methanol is inevitable, but we think that the effect of methanol evaporation during the SFG spectra acquisition can be negligible. The reasons are presented as follows.

Reason 1. The vapor pressure of 1 M methanol is sufficiently low that the evaporation of methanol can be considered negligible. It is well known that the vapor pressure of methanol on the 1 M methanol aqueous solution surface can be determined by Henry's Law. At a temperature of 293 K, the Henry Law constant of methanol in water is 20 kPa[25]. Consequently, the calculated vapor pressure of 1 M methanol solution with a molar fraction of only 0.018 is merely 0.36 kPa, indicating an extremely low level of methanol evaporation.

Reason 2. There are many literatures proved that the methanol evaporation caused by exposure time has no effect on the obtained SFG spectra at the neat methanol solution surface and the CH_3 orientation angle of interfacial methanol. For example, the IR absorption by methanol vapor was found to be less than 5% in Heather Allen's study[6]. The BBSFG spectrum from a neat methanol solution surface with exposure time of 2 min (Figure S4(c)) in this work is consistent with the BBSFG spectrum from neat methanol solution surface with exposure time of 1 min in Allen's work, and also agrees

with previously published spectra both from a closed sample cell[26] and an open cell to the laboratory atmosphere[8].

Reason 3. The orientation angle of methyl at surface of neat methanol in our study with exposure time of 2 min matches that reported in previously picosecond SFG-VS experiments in which the acquisition time usually took about 6 minutes to 80 minutes [16, 18, 19]. This indicates that the methanol evaporation caused by exposure time has no effect on the CH_3 orientation angle of interfacial methanol and the obtained SFG spectra at the neat methanol solution surface. Moreover, we found that the orientation angles of methyl at surface of 1 M methanol solution with the 10 min exposure time and 3 M methanol solution with the 2 min exposure time are both ~28° at the section 4 in supporting information. This further indicates that the methanol evaporation caused by exposure time has no effect on the CH_3 orientation angle of interfacial methanol at 1 M methanol aqueous solution surface.

Reason 4. Further, the exposure time of 1 M CH_3OH+0.1 M $NaClO_4$, 1 M CH_3OH+0.1 M $HClO_4$ and 1 M CH_3OH solutions is 10 min in Figure 1(a), 3 min in Figure S1(a) and 10 min in Figure S2(b), respectively. The spectra and fitting results of 3 min were consistent with the results of 10 min (Table S4, S5 and S7), that is, the oscillator strength of $CH_{3,\ SS}$ decreased at the surfaces of 0.1 M $NaClO_4$ solution and 0.1 M $HClO_4$ solution compared with the pure water surface. This indicates that the evaporation of methanol caused by exposure time has also no effect on the SFG spectra acquired at the electrolyte aqueous solution surface.

Combined all the analysis above, we conclude that methanol vapor has negligible impact on acquired SFG spectra. The variations in oscillator strength of methanol observed on the surface of different solutions through fitting SFG signals are attributed to differences in molecular relative number density or orientation angle.

9. The fitting parameters

Table S4. The fitting parameters of Figure 1(a) and S4(b).

Liquid	$A_q/a.u.$	ω_q/cm^{-1}	Γ_q/cm^{-1}	$Re[\chi_{NR}]$	$Im[\chi_{NR}]$

1 M CH_3OH	SSP	19.6±0.1	2839.6±0.1	10.9±0.1	-0.91±0.004	0.07±0.01
	PPP	-7.0±0.7	2840.9±1.3	13.6±1.5	-0.13±0.02	0
0.1 M $HClO_4$ +1 M CH_3OH	SSP	18.0±0.1	2839.6±0.1	10.6±0.1	-0.91±0.004	-0.03±0.01
	PPP	-6.9±0.6	2840.0±1.0	12.6±1.2	-0.13±0.02	0
0.1 M $NaClO_4$ +1 M CH_3OH	SSP	19.1±0.1	2839.9±0.1	10.8±0.1	-0.80±0.005	0.10±0.01
	PPP	-5.2±0.5	2837.8±0.8	10.9±1.2	-0.20±0.01	0

Table S5. The fitting parameters of Figure S1(a).

Liquid	$A_q/a.u.$	ω_q/cm^{-1}	Γ_q/cm^{-1}	$Re[\chi_{NR}]$	$Im[\chi_{NR}]$
1 M CH_3OH	12.9±0.2	2840.2±0.1	10.0±0.2	-0.57±0.01	0
0.1 M $HClO_4$ +1 M CH_3OH	12.2±0.2	2840.5±0.1	10.1±0.2	-0.58±0.01	0
0.1 M $NaClO_4$ +1 M CH_3OH	12.5±0.2	2840.1±0.1	9.9±0.2	-0.46±0.01	0

Table S6. The fitting parameters of Figure 3(a) and Figure S5.

Liquid	$A_q/a.u.$	ω_q/cm^{-1}	Γ_q/cm^{-1}	$Re[\chi_{NR}]$	$Im[\chi_{NR}]$
pure water	5.6±0.6	3248.9±6.4	120.0±0.0	-0.07±0.004	0.001±0
0.1 M $HClO_4$	7.3±0.6	3249.5±5.1	120.0±0.0	-0.07±0.004	0.001±0
0.1 M $NaClO_4$	1.0±0.1	3235.7±4.7	50.0±0.0	-0.06±0.002	0.001±0
1 M CH_3OH	10.7±0.3	3263.5±3.1	100.0±0.0	-0.03±0.003	0.001±0
0.1 M $HClO_4$ +1 M CH_3OH	11.7±0.3	3251.7±2.8	100.0±0.0	-0.02±0.003	0.001±0
0.1 M $NaClO_4$ +1 M CH_3OH	6.2±0.2	3265.3±3.4	80.0±0.0	-0.02±0.002	0.001±0

Table S7. The fitting parameters of Figure S2(b).

Liquid	$A_q/a.u.$	ω_q/cm^{-1}	Γ_q/cm^{-1}	$Re[\chi_{NR}]$	$Im[\chi_{NR}]$
1 M CH_3OH	20.8±0.2	2841.5±0.1	10.7±0.1	-0.84±0.01	0
0.1 M $HClO_4$ +1 M CH_3OH	19.8±0.2	2841.6±0.1	10.7±0.1	-0.85±0.01	0

0.1 M $NaClO_4$ +1 M CH_3OH	20.1±0.5	2840.4±0.1	11.6±0.2	-0.66±0.02	0

Table S8. The fitting parameters of Figure S4(c) and S4(d).

Liquid		$A_q/a.u.$	ω_q/cm^{-1}	Γ_q/cm^{-1}	$Re[\chi_{NR}]$	$Im[\chi_{NR}]$
Neat	SSP	27.2±0.2	2832.9±0.08	11.4±0.09	-0.47±0.007	-0.25±0.01
	PPP	-9.9±0.7	2835.8±1.0	12.1±1.0	-0.1±0.02	0
3 M	SSP	21.8±0.2	2838.5±0.1	10.9±0.1	-0.49±0.007	-0.16±0.02
	PPP	-7.7±0.8	2840.8±1.3	11.8±1.4	-0.12±0.02	0

References:

1. H.-t. Bian, R.-r. Feng, Y.-y. Xu, Y. Guo and H.-f. Wang, *Phys. Chem. Chem. Phys.*, 2008, **10**, 4920-4931.
2. E. H. G. Backus, D. Bonn, S. Cantin, S. Roke and M. Bonn, *J. Phys. Chem. B*, 2012, **116**, 2703-2712.
3. G. M. Hale and M. R. Querry, *Appl. Opt.*, 1973, **12**, 555-563.
4. B. Choi and A. J. Welch, *Lasers Surg. Med.*, 2001, **29**, 351-359.
5. Y. Xu, R. Wang, S. Ma, L. Zhou, Y. R. Shen and C. Tian, *J. Appl. Phys.*, 2018, **123**, 025301.
6. G. Ma and H. C. Allen, *J. Phys. Chem. B*, 2003, **107**, 6343-6349.
7. J. Hou, G. Sun, J. Liu, X. Gao, X. Zhang and Z. Lu, *J. Phys. Chem. B*, 2020, **124**, 4211-4221.
8. R. Superfine, J. Y. Huang and Y. R. Shen, *Phys. Rev. Lett.*, 1991, **66**, 1066-1069.
9. H. Chen, W. Gan, R. Lu, Y. Guo and H.F. Wang, *J. Phys. Chem. B*, 2005, **109**, 8064-8075.
10. R. Lu, W. Gan, B.-h. Wu, Z. Zhang, Y. Guo and H.-f. Wang, *J. Phys. Chem. B*, 2005, **109**, 14118-14129.
11. J. Sung, K. Park and D. Kim, *J. Phys. Chem. B*, 2005, **109**, 18507-18514.
12. X. Li, J. Liu, K. Lin, Y. Zhang, Y. Zhang, R. Zheng, Q. Shi, Y. Guo and Z. Lu, *J. Phys. Chem. C*, 2019, **123**, 12975-12983.

13. X. Zhuang, P. B. Miranda, D. Kim and Y. R. Shen, *Phys. Rev. B*, 1999, **59**, 12632-12640.
14. M. J. Colles and J. E. Griffiths, *J. Chem. Phys.*, 1972, **56**, 3384-3391.
15. D. Zhang, J. Gutow and K. B. Eisenthal, *J. Phys. Chem.*, 1994, **98**, 13729-13734.
16. K. Wolfrum, H. Graener and A. Laubereau, *Chem. Phys. Lett.*, 1993, **213**, 41-46.
17. H.F. Wang, W. Gan, R. Lu, Y. Rao and B.H. Wu, *Int. Rev. Phys. Chem.*, 2005, **24**, 191-256.
18. W. Gan, B.H. Wu, H. Chen, Y. Guo and H.F. Wang, *Chem. Phys. Lett.*, 2005, **406**, 467-473.
19. X. Li, G.H. Deng, R.J. Feng, K. Lin, Z. Zhang, Y. Bai, Z. Lu and Y. Guo, *Chin. Chem. Lett.*, 2016, **27**, 535-539.
20. M. Matsumoto and Y. Kataoka, *J. Chem. Phys.*, 1989, **90**, 2398-2407.
21. P. E. Ohno, H. Chang, A. P. Spencer, Y. Liu, M. D. Boamah, H.-f. Wang and F. M. Geiger, *J. Phys. Chem. Lett.*, 2019, **10**, 2328-2334.
22. E. Ma, P. E. Ohno, J. Kim, Y. Liu, E. H. Lozier, T. F. Miller, H.-F. Wang and F. M. Geiger, *J. Phys. Chem. Lett.*, 2021, **12**, 5649-5659.
23. R. Bai, Y. Lin, Y. Guo and Z. Zhang, *J. Chem. Phys.*, 2022, **156**, 234704.
24. P. K. Weissenborn and R. J. Pugh, *J. Colloid Interface Sci.*, 1996, **184**, 550–563
25. C. E. O'Farrell and W. E. Waghorne, *J. Chem. Eng. Data*, 2010, **55**, 1655-1658.
26. C. D. Stanners, Q. Du, R. P. Chin, P. Cremer, G. A. Somorjai and Y.-R. Shen, *Chem. Phys. Lett.*, 1995, **232**, 407-413.